Hypersonic drift-tearing magnetic islands in tokamak plasmas

R. Fitzpatrick and F. L. Waelbroeck
Institute for Fusion Studies, Department of Physics, University of Texas at Austin, Austin, Texas 78712, USA

A two-fluid theory of long wavelength, hypersonic, drift-tearing magnetic islands in low-collisionality, low-β plasmas possessing relatively weak magnetic shear is developed. The model assumes both slab geometry and cold ions, and neglects electron temperature and equilibrium current gradient effects. The problem is solved in three asymptotically matched regions. The "inner region" contains the island. However, the island emits electrostatic drift-acoustic waves that propagate into the surrounding "intermediate region," where they are absorbed by the plasma. Since the waves carry momentum, the inner region exerts a net force on the intermediate region, and vice versa, giving rise to strong velocity shear in the region immediately surrounding the island. The intermediate region is matched to the surrounding "outer region," in which ideal magnetohydrodynamic holds. Isolated hypersonic islands propagate with a velocity that lies between those of the unperturbed local ion and electron fluids, but is much closer to the latter. The ion polarization current is *stabilizing*, and *increases* with increasing island width. Finally, the hypersonic branch of isolated island solutions *ceases to exist* above a certain critical island width. Hypersonic islands whose widths exceed the critical width are hypothesized to bifurcate to the so-called "sonic" solution branch. © *2007 American Institute of Physics.* [DOI: 10.1063/1.2811928]

I. INTRODUCTION

Tearing modes[1] are slowly growing macroscopic plasma instabilities that often limit fusion plasma performance in magnetic confinement devices, such as tokamaks, which rely on nested toroidal magnetic flux surfaces.[2] As the name suggests, "tearing" modes tear and reconnect magnetic field-lines, in the process converting nested toroidal flux surfaces into nonaxisymmetric configurations containing rotating chains of narrow (in the radial direction) helical magnetic islands.[3] Such islands degrade plasma confinement because heat and particles are able to travel radially from one side of an island to another by flowing along magnetic field-lines, which is a relatively fast process, instead of having to diffuse across magnetic flux surfaces, which is a relatively slow process.[4] It is therefore important for fusion scientists to gain a thorough understanding of the physics of magnetic islands—particularly of those factors that cause such islands to either grow or decay. Furthermore, given the macroscopic nature of magnetic islands, and their relatively weak time dependence, it is natural to investigate them using some form of fluid theory.[5–8]

As is well known, the simple single-fluid magnetohydrodynamical (MHD) closure of plasma fluid equations leads to a relatively poor description of slowly growing macroscopic instabilities in the high-temperature plasmas typically found in modern-day tokamaks.[9–12] A far better description is obtained using the more complicated two-fluid drift-MHD closure.[11,12] Recent research has established that there are two main classes of magnetic island solutions within the context of two-fluid drift-MHD theory. *Sonic* island solutions are characterized by a flattened electron number density profile within the magnetic separatrix, a relatively large radial width, a propagation velocity close to that of the unperturbed

local ion fluid, and a relatively weak coupling to drift-acoustic waves.[13–16] On the other hand, *hypersonic* island solutions are characterized by a nonflattened density profile within the magnetic separatrix, a relatively small radial width, a propagation velocity close to that of the unperturbed local electron fluid, and a relatively strong coupling to drift-acoustic waves.[13–15] Recent computer simulations suggest that the sonic branch of solutions ceases to exist below some critical island width, whereas the hypersonic branch ceases to exist above a second, somewhat larger, critical width.[13,14] The disappearance of one branch of solutions is associated with a bifurcation to the other branch.[13,14]

This paper is concerned with the *hypersonic* branch of island solutions. Employing a reduced *four-field model*[17] of the plasma dynamics, and building on previous results,[18–20] a semi-analytic theory is developed that exploits the peculiar properties of hypersonic islands. The main aims of this theory are, firstly, to determine the island propagation velocity relative to the local ion and electron fluids, secondly, to find the magnitude and sign of the ion polarization term appearing in the Rutherford island width evolution equation,[3,7] and thirdly, to determine whether there exists a critical island width above which the hypersonic branch of solutions ceases to exist.

II. FOUR-FIELD MODEL

A. Introduction

Consider a *steady-state* magnetic island in two-dimensional *slab geometry*. The magnetic field in the vicinity of the island is assumed to be dominated by a uniform constant guide-field directed along the z axis. Furthermore, $\partial/\partial z \equiv 0$. Equilibrium quantities vary in the x direction only. All mean flows are in the y direction. The system is periodic

14, 122502-1

in the y direction, with periodicity length L_y. The electron temperature takes the constant value T_e. The ions are cold (compared to the electrons) and singly charged. Finally, there is a uniform equilibrium density gradient, a uniform z-directed equilibrium current density (generating a sheared equilibrium B_y that passes through zero at $x=0$), and zero shear in the equilibrium $\mathbf{E} \times \mathbf{B}$ velocity.

B. Normalization

For the sake of clarity, we initially adopt a conventional normalization scheme. Hence, all lengths are normalized to the magnetic shear length L_s (i.e., the gradient scale-length of the equilibrium B_y). All magnetic field strengths are normalized to that of the guide field B_z (which is equivalent to the equilibrium value of B_y at $|x|=L_s$). Finally, all times are normalized to the shear-Alfvèn time $\tau_A = L_s \sqrt{\mu_0 n_{e0} m_i}/B_z$, and all velocities to the shear-Alfvèn velocity $V_A = L_s/\tau_A$. Here, n_{e0} is the background electron number density, and m_i the ion mass.

C. Model equations

In the island rest frame ($\partial/\partial t \equiv 0$), the (conventionally normalized) "four-field" equations take the familiar form[17]

$$0 = [\phi - n, \psi] + \eta J, \tag{1}$$

$$0 = [\phi, n] + [V + \rho^2 J, \psi] + D \nabla^2 n, \tag{2}$$

$$0 = [\phi, U] + [J, \psi] + \mu \nabla^2 U, \tag{3}$$

$$0 = [\phi, V] + \beta[n, \psi] + \chi \nabla^2 V, \tag{4}$$

$$U = \nabla^2 \phi, \tag{5}$$

$$J = 1 + \nabla^2 \psi, \tag{6}$$

where

$$[A, B] \equiv \nabla A \times \nabla B \cdot \hat{\mathbf{z}}. \tag{7}$$

Here, $\psi = A_z/B_z L_s$, $\phi = -\Phi/B_z L_s V_A$, $n = -\sqrt{\beta}\rho(\delta n_e/n_{e0})$, and $V = \sqrt{\beta}\rho(V_{zi}/V_A)$, where A_z is the z component of the magnetic vector potential, Φ the electric scalar potential, δn_e the perturbed electron number density, and V_{zi} the z component of the ion fluid velocity. Moreover, ρ is the (normalized) ion sonic radius, whereas β is (half) the plasma beta. [In other words, $\rho = \rho_s/L_s$ and $\beta = \mu_0 n_{e0} T_e/B_z^2$, where $\rho_s = (T_e/m_i)^{1/2}/(eB_z/m_i)$ and e is the magnitude of the electron charge.] Finally, η is the (normalized) plasma resistivity, D the (normalized) perpendicular particle diffusivity, μ the (normalized) perpendicular ion viscosity, while χ parametrizes the effect of ion-ion collisions on the parallel flow. (Note that the true parallel ion viscosity is neglected in the above equations.) The parameters η, D, μ, χ, ρ, and β are all assumed to be uniform constants.

D. Boundary conditions

The following tearing parity constraints are adopted for the various fields appearing in Eqs. (1)–(6): ψ, J, and V are even in x, whereas ϕ, U, and n are odd. This implies that $\partial \psi/\partial x = \partial J/\partial x = \partial V/\partial x = \phi = U = n = 0$ at $x=0$. The boundary conditions at large $|x|$ are

$$\partial n/\partial x \rightarrow -V_*, \tag{8}$$

$$\partial \phi/\partial x \rightarrow -V_*(1 + v_\infty + v'_\infty|x|), \tag{9}$$

$$\partial U/\partial x, J, V \rightarrow 0, \tag{10}$$

$$\psi \rightarrow -\tfrac{1}{2}x^2 + w^2 \cos \theta. \tag{11}$$

Here, $V_* = \rho\sqrt{\beta}(L_s/L_n)$ is the (normalized) electron diamagnetic velocity, L_n the equilibrium density gradient scale-length (which is assumed to be much less than L_s), and $\theta = ky$, where $k = 2\pi(L_s/L_y)$. Moreover, v_∞ is termed the "asymptotic slip-velocity," and v'_∞ the "asymptotic slip-velocity gradient." The asymptotic slip-velocity measures the deviation of the island propagation velocity from that of the unperturbed local electron fluid, whereas the asymptotic slip-velocity gradient parametrizes the net external force acting on the island region (which is proportional to $\mu v'_\infty$). Of course, the net external force is *zero* for an *isolated* island that is not interacting with an external magnetic perturbation or a resistive wall.[21] Finally, the quantity w measures the (normalized) island width in the x direction (assuming that the island is constant-ψ).

E. Renormalization

We are interested in island solutions for which $w \sim \rho$. We also expect all (normalized) velocities in our problem to be of order V_*. It is therefore convenient to renormalize our equations such that $x = \rho\hat{x}$, $w = \rho\hat{w}$, $v'_\infty = \hat{v}'_\infty/\rho$, $\phi = \rho V_*\hat{\phi}$, $n = \rho V_*\hat{n}$, $U = (V_*/\rho)\hat{U}$, $J = (V_*/\rho)^2\hat{J}$, $\psi = \rho^2\hat{\psi}$, $V = V_*^2\hat{V}$, $C = \hat{\beta}(\eta/\rho^2 kV_*)$, $\hat{D} = (D/\rho^2 kV_*)$, $\hat{\mu} = (\mu/\rho^2 kV_*)$, $\hat{\chi} = (\chi/\rho^2 kV_*)$, and

$$\hat{\beta} = \frac{\beta}{\epsilon_n^2}, \tag{12}$$

$$\epsilon_n = \frac{L_n}{L_s}. \tag{13}$$

Here, C is the well-known collisionality parameter of Drake *et al.*[22] It follows that our renormalized equations take the form

$$0 = [\hat{\phi} - \hat{n}, \hat{\psi}] + C\hat{J}, \tag{14}$$

$$0 = [\hat{\phi}, \hat{n}] + [\hat{V} + \hat{J}, \hat{\psi}] + \hat{D}\nabla^2\hat{n}, \tag{15}$$

$$0 = [\hat{\phi}, \hat{U}] + [\hat{J}, \hat{\psi}] + \hat{\mu}\nabla^2\hat{U}, \tag{16}$$

$$0 = [\hat{\phi}, \hat{V}] + \epsilon_n^2[\hat{n}, \hat{\psi}] + \hat{\chi}\nabla^2\hat{V}, \tag{17}$$

$$\hat{U} = \nabla^2 \hat{\phi}, \tag{18}$$

$$\nabla^2 \hat{\psi} = -1 + \hat{\beta}\hat{J}, \tag{19}$$

where

$$[A,B] \equiv A_x B_\theta - A_\theta B_x, \tag{20}$$

$$\nabla^2 A \equiv A_{xx} + (k\rho)^2 A_{\theta\theta}. \tag{21}$$

Here, the subscripts x and θ denote $\partial/\partial\hat{x}$ and $\partial/\partial\theta$, respectively. Note that the system is periodic in θ, with period 2π. The boundary conditions at $\hat{x}=0$ are $\psi_x = J_x = V_x = \phi = n = U = 0$, whereas the boundary conditions at $|\hat{x}| \to \infty$ become

$$\hat{n}_x \to -1, \tag{22}$$

$$\hat{\phi}_x \to -1 - v_\infty - \hat{v}'_\infty |\hat{x}|, \tag{23}$$

$$\hat{U}_x, \hat{J}, \hat{V} \to 0, \tag{24}$$

$$\hat{\psi} \to -\tfrac{1}{2}\hat{x}^2 + \hat{w}^2 \cos\theta. \tag{25}$$

F. Ordering scheme

The primary ordering scheme adopted in this paper is

$$1 \gg \hat{\beta} \tag{26}$$

and

$$1 \gg \epsilon_n^2 \gg \hat{D}, \hat{\mu}, \hat{\chi} \gg C. \tag{27}$$

This is equivalent to a large-aspect-ratio, low-beta, low-collisionality ordering in which the island is much wider than a typical drift-tearing linear layer.

Equations (19), (25), and (26) yield

$$\hat{\psi}(\hat{x}, \theta) = -\tfrac{1}{2}\hat{x}^2 + \hat{w}^2 \cos\theta + O(\hat{\beta}). \tag{28}$$

In other words, our ordering scheme implies the well-known "constant-ψ approximation."[3] It follows, from Eq. (28), that the magnetic separatrix lies at $|\hat{x}| = 2\hat{w}\cos(\theta/2)$, and thus that the island width parameter $\hat{w}$ represents one quarter of the (renormalized) full separatrix width (in the $\hat{x}$ direction). The region inside the separatrix corresponds to $\hat{\psi} > -\hat{w}^2$, whereas the region outside the separatrix corresponds to $\hat{\psi} < -\hat{w}^2$.

We also adopt the long-wavelength ordering

$$k\rho \ll 1, \tag{29}$$

which implies that

$$\nabla^2 A \simeq A_{xx}. \tag{30}$$

G. Overview of solution

We shall solve our problem in three asymptotically matched regions. The "inner region" extends over $|\hat{x}| \ll \epsilon_n^{-1/2}$, whereas the "intermediate region" extends over $|\hat{x}| \gg \hat{w}$. Our island solution is matched to a conventional ideal-MHD solution at the edge of the intermediate region.[1,3] The inner region contains the island, and is thus *nonlinear*. However,

the intermediate region is *linear*. In fact, the magnetic island acts as an "antenna" that radiates drift-acoustic waves into the intermediate region, where they are absorbed by the plasma.[15,19] These waves carry momentum, giving rise to a net exchange of momentum between the two regions.

III. INNER REGION

A. Basic equations

Temporarily neglecting hats, for the sake of clarity, and making use of the ordering assumptions introduced in Sec. II F, the renormalized equations (14)–(19) reduce to

$$0 = [\phi - n, \psi] + CJ, \tag{31}$$

$$0 = [\phi, n] + [V + J, \psi] + Dn_{xx}, \tag{32}$$

$$0 = [\phi, U] + [J, \psi] + \mu U_{xx}, \tag{33}$$

$$0 = [\phi, V] + \epsilon_n^2[n, \psi] + \chi V_{xx}, \tag{34}$$

$$\phi_{xx} = U, \tag{35}$$

$$\psi = -\tfrac{1}{2}x^2 + w^2 \cos\theta \tag{36}$$

in the inner region; i.e., $|x| \ll \epsilon_n^{-1/2}$.

Let

$$\phi = -x + \delta\phi, \tag{37}$$

$$n = -x + \delta n. \tag{38}$$

It is easily seen that if $w \sim O(1)$, then our ordering scheme requires that

$$\psi \sim O(1), \tag{39}$$

$$\delta\phi, \delta n, V, U, J \sim O(\epsilon_n^2). \tag{40}$$

The boundary conditions at large $|x|$ are

$$\overline{\delta\phi}_x \to -v_i - v'_i |x|, \tag{41}$$

$$\overline{\delta n}_x, \overline{U}_x, \overline{V}, \overline{J} \to 0, \tag{42}$$

where $\overline{(\cdots)}$ denotes an average over θ at constant x. Here, the constants v_i and v'_i are the asymptotic slip-velocity and slip-velocity gradient, respectively, at the edge of the inner region. Note that these are not necessarily the same as the corresponding quantities at the edge of the intermediate region, because of the momentum exchange between the two regions.

B. Analysis

To lowest order in ϵ_n^2, Eqs. (31)–(35) give

$$0 = [\delta\phi - \delta n, \psi] + CJ, \tag{43}$$

$$0 = [\delta n - \delta\phi, x] + [V + J, \psi] + D\delta n_{xx}, \tag{44}$$

$$0 = [U, x] + [J, \psi] + \mu U_{xx}, \tag{45}$$

$$0 = [V + \epsilon_n^2 \psi, x] + \chi V_{xx}, \tag{46}$$

with $U = \delta\phi_{xx}$. Each of the above equations yields an equilibrium constraint (obtained by neglecting transport terms) and a solubility condition, obtained by averaging away all terms except transport terms.

Equation (46) gives the equilibrium constraint

$$V = -\epsilon_n^2 w^2 \cos\theta + F(x), \tag{47}$$

and the solubility condition

$$F_{xx} = 0. \tag{48}$$

The only even (in x) solution of the above equation that satisfies the boundary condition $\bar{V} \to 0$ at large $|x|$ is

$$F = 0. \tag{49}$$

Hence,

$$V = -\epsilon_n^2 w^2 \cos\theta. \tag{50}$$

Equation (43) gives the equilibrium constraint

$$\delta n = \delta\phi + H(\psi), \tag{51}$$

plus the solubility condition

$$\langle J \rangle = 0. \tag{52}$$

Here, the flux-surface average operator $\langle \cdots \rangle$ is defined as[3]

$$
\langle f(s, \psi, \theta) \rangle
$$
$$
\equiv
\begin{cases}
\displaystyle\oint \frac{f(s, \psi, \theta)}{|x|} \frac{d\theta}{2\pi}, & \psi \leq -w^2, \\[2ex]
\displaystyle\int_{-\theta_0}^{\theta_0} \frac{f(s, \psi, \theta) + f(-s, \psi, \theta)}{2|x|} \frac{d\theta}{2\pi}, & \psi > -w^2,
\end{cases}
\tag{53}
$$

where $s = \mathrm{sgn}(x)$, $x(s, \psi, \theta_0) = 0$, and the integrals are performed at constant ψ.

Equation (44) can be written

$$0 = [-H'x - \epsilon_n^2 w^2 \cos\theta + J, \psi] + D(\delta\phi_{xx} + H_{xx}) + O(C), \tag{54}$$

where $'$ denotes $d/d\psi$. This expression, combined with the solubility condition (52), yields the equilibrium constraint

$$J = H'\tilde{x} + \frac{\epsilon_n^2}{2} \widetilde{x^2}, \tag{55}$$

as well as the solubility condition

$$\langle \delta\phi_{xx} + H_{xx} \rangle = 0. \tag{56}$$

Here,

$$\tilde{f} \equiv f - \langle f \rangle / \langle 1 \rangle. \tag{57}$$

Finally, Eqs. (44) and (45) can be combined to give

$$0 = [U - H - \epsilon_n^2 w^2 x \cos\theta, x] + \mu U_{xx} - D(\delta\phi_{xx} + H_{xx})$$
$$+ O(C). \tag{58}$$

This equation yields the equilibrium constraint

$$U = \delta\phi_{xx} = H(\psi) + K(x) + \epsilon_n^2 w^2 x \cos\theta, \tag{59}$$

and the solubility condition

$$0 = \mathrm{Sc}^{-1}(\overline{\delta\phi_{xx}} + \bar{H}_{xx}) - (\bar{H}_{xx} + K_{xx}), \tag{60}$$

where $\mathrm{Sc} = \mu/D$ is the so-called "Schmidt number."[16]

C. Determination of profile functions

The unknown profile functions $H(\psi)$ and $K(x)$, are determined by the solubility conditions (56) and (60), respectively.

Equation (56) can be written

$$\frac{d}{d\psi}(\langle x^2 \rangle H' + \langle xv \rangle) = 0, \tag{61}$$

where

$$v = -\delta\phi_x. \tag{62}$$

Integration yields

$$
H'(\psi) =
\begin{cases}
-s\left(\dfrac{\langle xv \rangle + v_c}{\langle x^2 \rangle}\right), & \psi \leq -w^2, \\[2ex]
0, & \psi > -w^2,
\end{cases}
\tag{63}
$$

since $H(\psi)$ is an odd function of x, and must therefore be zero inside the magnetic separatrix. Here, v_c is a constant.

Integration of Eq. (60), making use of the boundary conditions $\overline{\delta n}_x, \bar{U}_x \to 0$ as $|x| \to \infty$, gives

$$K_x = x\bar{H}' - \mathrm{Sc}^{-1}(\bar{v} + x\bar{H}'). \tag{64}$$

Finally, taking the x-derivative of Eq. (59), we obtain

$$v_{xx} = xH' - K_x - \epsilon_n^2 w^2 \cos\theta \tag{65}$$

or

$$v_{xx} = \mathrm{Sc}^{-1}(\bar{v} - \bar{G}) - (G - \bar{G}) - \epsilon_n^2 w^2 \cos\theta, \tag{66}$$

where

$$
G = -xH' =
\begin{cases}
|x|\left(\dfrac{\langle xv \rangle + v_c}{\langle x^2 \rangle}\right), & \psi \leq -w^2, \\[2ex]
0, & \psi > -w^2.
\end{cases}
\tag{67}
$$

It remains to determine the constant v_c. Now, at large $|x|$, we expect

$$H'(\psi) \to s[h_1 + h_0(-2\psi)^{-1/2} + O(\psi^{-1})] \tag{68}$$

and

$$G = -xH' \to -h_1|x| - h_0 + O(x^{-1}). \tag{69}$$

Thus, substituting into Eq. (66), and making use of the boundary condition (41), we obtain

$$v_{xx} \to \mathrm{Sc}^{-1}[v_i + h_0 + (v_i' + h_1)|x|] - \epsilon_n^2 w^2 \cos\theta + O(x^{-1}). \tag{70}$$

The boundary condition (41) can only be satisfied if $h_0 = -v_i$, and $h_1 = -v_i'$. Hence,

$$v \to v_i + v_i'|x| - \frac{\epsilon_n^2}{2} w^2 x^2 \cos \theta \qquad (71)$$

as $|x| \to \infty$. Now, since $-x^2/2 = \psi - w^2 \cos \theta$, and a flux-surface average is carried out at constant ψ, we can write

$$\langle xv \rangle \to v_i + v_i'|x| + \epsilon_n^2 w^2 \overline{(\psi - w^2 \cos \theta) \cos \theta} + O(x^{-1}), \qquad (72)$$

which reduces to

$$\langle xv \rangle \to v_i + v_i'|x| - \frac{\epsilon_n^2 w^4}{2}. \qquad (73)$$

Thus, it follows from Eqs. (67) and (69) that

$$v_c = \frac{\epsilon_n^2 w^4}{2}. \qquad (74)$$

D. Final scheme

Our final system of equations in the inner region is

$$v_{xx} = \mathrm{Sc}^{-1}(\bar{v} - \bar{G}) - (G - \bar{G}) - \epsilon_n^2 w^2 \cos \theta, \qquad (75)$$

and

$$G = \begin{cases} |x| \left(\dfrac{\langle xv \rangle + \epsilon_n^2 w^4/2}{\langle x^2 \rangle} \right), & \psi \leqslant -w^2, \\ 0, & \psi > -w^2, \end{cases} \qquad (76)$$

subject to the boundary conditions

$$v_x = 0 \qquad (77)$$

at $x=0$, and

$$v \to v_i + v_i'|x| - \frac{\epsilon_n^2}{2} w^2 x^2 \cos \theta \qquad (78)$$

as $|x| \to \infty$. Of course, $v(x, \theta)$ is periodic in θ, with period 2π. Recall that $\langle \cdots \rangle$ denotes a flux-surface average [see Eq. (53)], whereas $\overline{(\cdots)}$ denotes a θ average at constant x. The above equations can be solved via iteration. Note that (with ϵ_n, w, and Sc fixed) the solution to our inner region equations contains only a single free parameter, which can be taken to be the value of $\bar{v}$ at $x=0$.

The current density in the inner region is written

$$J = -\tilde{G} + \frac{\epsilon_n^2}{2} \widetilde{x^2}. \qquad (79)$$

Observe that J does not go to zero as $|x| \to \infty$, as is necessary in order to match our island solution to a conventional ideal-MHD solution at very large $|x|$. It follows that there must exist a region (termed the "intermediate region") sandwiched between the inner and the ideal-MHD regions, in which J decays to zero.

Note, finally, that

$$\delta n_x = G - v \to \frac{\epsilon_n^2}{2} w^2 x^2 \cos \theta \qquad (80)$$

as $|x| \to \infty$.

IV. INTERMEDIATE REGION

A. Linearization

The intermediate region extends over $|\hat{x}| \gg \hat{w}$. It follows that we can linearize Eqs. (14)–(19) in this region. Again temporarily neglecting hats, for the sake of clarity, we can write

$$\phi(x, \theta) = -x + \overline{\delta\phi}(x) + \check{\phi}(x) e^{i\theta}, \qquad (81)$$

$$n(x, \theta) = -x + \check{n}(x) e^{i\theta}, \qquad (82)$$

$$U(x, \theta) = \bar{U}(x) + \check{U}(x) e^{i\theta}, \qquad (83)$$

$$V(x, \theta) = \check{V}(x) e^{i\theta}, \qquad (84)$$

$$J(x, \theta) = \check{J}(x) e^{i\theta}, \qquad (85)$$

$$\psi(x, \theta) = -\tfrac{1}{2} x^2 + w^2 e^{i\theta}, \qquad (86)$$

where all "$\check{\ }$" terms are of first order [i.e., $O(w^2/x^2)$]. The absence of a $\overline{\delta n}(x)$ term in Eq. (82) is consistent with the asymptotic behavior of δn at the edge of the inner region exhibited in Eq. (80).

Neglecting the transport terms, linearization of Eqs. (14)–(19) yields

$$x\check{J} = (\bar{v} - \epsilon_n^2 x^2) \left(\check{\phi} - \frac{w^2}{x} \right), \qquad (87)$$

$$\check{\phi}_{xx} = \bar{v}_{xx} \check{\phi} + x\check{J}, \qquad (88)$$

which give

$$\check{\phi}_{xx} - \bar{v}_{xx} \check{\phi} - (\bar{v} - \epsilon_n^2 x^2) \check{\phi} = -(\bar{v} - \epsilon_n^2 x^2) \frac{w^2}{x} \qquad (89)$$

and

$$\check{J} = \frac{\check{\phi}_{xx} - \bar{v}_{xx} \check{\phi}}{x}, \qquad (90)$$

where $\bar{v}(x) = -\overline{\delta\phi}_x(x)$. Here, it is assumed that $|\bar{v}| \ll 1$. Equation (89) is solved subject to the boundary conditions

$$\check{\phi} \to 0 \qquad (91)$$

as $x \to 0$, and

$$\check{\phi} \to \frac{w^2}{x} \qquad (92)$$

as $|x| \to \infty$. It follows from Eq. (90) that

$$\check{J} \to 0 \qquad (93)$$

as $|x| \to \infty$. (Here, we assume that $\bar{v}_{xx} \to 0$ as $|x| \to \infty$, since there is no equilibrium velocity shear.) Equations (92) and (93) demonstrate that the island solution in the intermediate region can be successfully matched to an ideal-MHD solution at very large $|x|$. (The conventional linear ideal-MHD solution to the problem is simply $\check{J} = 0$ and $\check{\phi} = w^2/x$.[1,3])

B. Damping of drift-acoustic waves

Equation (89) is a driven wave equation that describes how electrostatic drift-acoustic waves[11,12] are excited by the island in the inner region, and then propagate into the intermediate region. In order to uniquely determine the solution in the intermediate region, we need to either adopt an "outgoing wave" boundary condition at large $|x|$,[23,24] or to add some form of wave damping to our model. It is more convenient to do the latter. Linearizing Eq. (16), and retaining the perpendicular viscosity, we obtain

$$\check{\phi}_{xx} + i\mu\check{\phi}_{xxxx} = \bar{v}_{xx} + x\check{J}. \tag{94}$$

However, it is clear from Eq. (89) that $\partial^2/\partial x^2 \to -\epsilon_n^2 x^2$ at large $|x|$. Hence, we get

$$\check{\phi}_{xx} \simeq \frac{\bar{v}_{xx}\check{\phi} + x\check{J}}{1 - i\mu\epsilon_n^2 x^2}. \tag{95}$$

This suggests that we should modify Eq. (89), by writing

$$\check{\phi}_{xx} - \bar{v}_{xx}\check{\phi} - \left(\bar{v} - \frac{\epsilon_n^2 x^2}{1 - i\mu\epsilon_n^2 x^2}\right)\check{\phi} = -\left(\bar{v} - \frac{\epsilon_n^2 x^2}{1 - i\mu\epsilon_n^2 x^2}\right)\frac{w^2}{x} \tag{96}$$

in order to mimic the damping effect of perpendicular viscosity on drift-acoustic waves at large $|x|$. Note that only those terms that are important at large $|x|$ have been modified. The boundary conditions remain the same. Strictly speaking, our analysis should also take into account the damping effect of the other transport coefficients D and χ (the effect of the collisionality parameter C is negligible, according to our ordering scheme). However, for the sake of simplicity, we shall neglect this additional damping.

C. Force balance

The mean velocity profile in the intermediate region, i.e., $\bar{v}(x)$, is determined from *quasilinear force balance*; i.e.,

$$0 = \frac{1}{2}\text{Im}(\check{\phi}_{xx}\check{\phi}_x^*) - \frac{w^2}{2}\text{Im}(\check{J}) + \mu\bar{v}_{xx}. \tag{97}$$

The first term on the right-hand side of the above equation represents the mean Reynolds stress force in the y direction, the second term the mean $\mathbf{j} \times \mathbf{B}$ force, and the third term the mean viscous force. Equations (96) and (97) can be combined to give

$$\bar{v}_{xx} = \frac{1}{2}\frac{\epsilon_n^4 x^2}{1 + (\mu\epsilon_n^2 x^2)^2}|w^2 - x\check{\phi}|^2. \tag{98}$$

This equation is solved subject to the boundary conditions

$$\bar{v} \to v_i + v_i'|x| \tag{99}$$

as $x \to 0$, and

$$\bar{v} \to v_\infty + v_\infty'|x| \tag{100}$$

as $|x| \to \infty$. Equation (98) describes how momentum carried by drift-acoustic waves radiated by the island is absorbed in the intermediate region, and modifies the mean velocity profile.

D. Final scheme

Our final system of equations in the intermediate region is

$$\check{\phi}_{xx} - \bar{v}_{xx}\check{\phi} - \left(\bar{v} - \frac{\epsilon_n^2 x^2}{1 - i\mu\epsilon_n^2 x^2}\right)\check{\phi}$$
$$= -\left(\bar{v} - \frac{\epsilon_n^2 x^2}{1 - i\mu\epsilon_n^2 x^2}\right)\frac{w^2}{x} \tag{101}$$

and

$$\bar{v}_{xx} = \frac{1}{2}\frac{\epsilon_n^4 x^2}{1 + (\mu\epsilon_n^2 x^2)^2}|w^2 - x\check{\phi}|^2. \tag{102}$$

The boundary conditions are

$$\check{\phi} \to 0, \tag{103}$$

$$\bar{v} \to v_i + v_i'|x| \tag{104}$$

as $x \to 0$, and

$$\check{\phi} \to \frac{w^2}{x}, \tag{105}$$

$$\bar{v} \to v_\infty + v_\infty'|x| \tag{106}$$

as $|x| \to \infty$. The perturbed current is given by

$$\check{J} = \frac{\check{\phi}_{xx} - \bar{v}_{xx}\check{\phi}}{x}. \tag{107}$$

The above set of equations can be solved via iteration.

V. OVERALL SOLUTION

The overall solution to our problem is obtained by generating a solution in the inner region, as described in Sec. III D, and then finding a matching solution in the intermediate region, as described in Sec. IV D. Note that, with $\hat{w}$, ϵ_n, $\hat{\mu}$, and Sc fixed, our overall solution contains a single free parameter, which can be taken to be the value of $\bar{v}$ at $x=0$. For an *isolated* island, which is not interacting with an external magnetic perturbation or a resistive wall, this free parameter is fixed by the *zero force constraint*[21]

$$v_\infty' = 0. \tag{108}$$

Hence, the inner and intermediate solutions described in Secs. III D and IV D, together with the above constraint, *uniquely* determine the island solution as a function of $\hat{w}$, ϵ_n, $\hat{\mu}$, and Sc.

It is helpful to define the parameter $v_0 = \bar{v}(0)$. The difference between the (normalized) mean ion and electron fluid flow velocities at the rational surface ($x=0$) is $V_*(1 + v_0)$. Hence, v_0 is a measure of the degree of density flattening inside the island, with $v_0 = 0$ corresponding to no flattening, and $v_0 = -1$ corresponding to complete flattening.

If V_p is the island phase velocity, V_e the unperturbed local electron fluid velocity, and V_i the unperturbed local ion fluid velocity, then
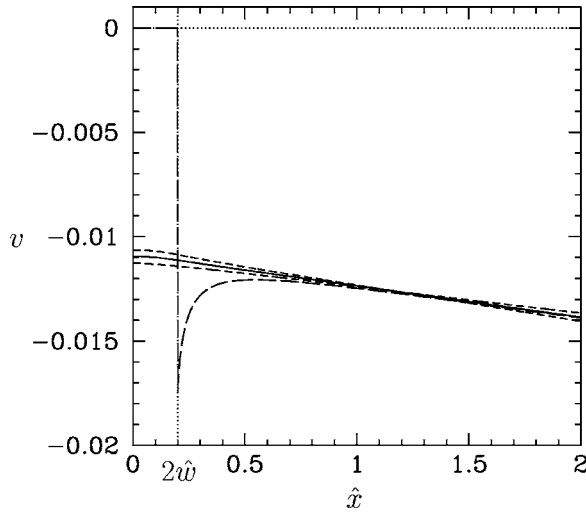
FIG. 1. Velocity profiles in the inner region for an isolated hypersonic island solution characterized by $\epsilon_n=0.1$, $\hat{\mu}=0.001$, Sc=1.0, and $\hat{w}=0.1$. The solid curve shows the mean ion fluid velocity profile $\bar{v}(\hat{x})$, whereas the short-dashed curves show the ion fluid velocity profile $v(\hat{x},\theta)$, through the island O- and X-points (i.e., at $\theta=0$ and π, respectively). The long-dashed curve shows the electron fluid velocity profile $G(\hat{x},\theta)$ through the island O-point.

$$\frac{V_p - V_e}{V_e - V_i} = v_\infty. \tag{109}$$

Observe that if v_∞ is negative (as will turn out to be the case), then the island phase velocity lies between those of the unperturbed local electron and ion fluid velocities. However, our ordering scheme ensures that $|v_\infty| \ll 1$. Hence, the island still propagates with a velocity which is much closer to that of the unperturbed local electron fluid than the unperturbed local ion fluid, as one would expect for a hypersonic island.

Finally, the Rutherford island width evolution equation takes the form[3,7]

$$\frac{dw}{dt} \propto \Delta'\rho_s + \frac{\beta}{\epsilon_n^2 \hat{w}^2} J_c, \tag{110}$$

where Δ' is the linear tearing stability index,[1] and

$$J_c = \int_0^\infty K_c(\hat{x})d\hat{x}, \tag{111}$$

with

$$K_c = \begin{cases} -(2/\pi)\oint [-\widetilde{G} + (\epsilon_n^2/2)\widetilde{\hat{x}^2}]\cos\theta d\theta, & \hat{x} \le \hat{x}_c, \\ -2\,\mathrm{Re}(\breve{J}), & \hat{x} > \hat{x}_c. \end{cases} \tag{112}$$

Here, $1 \ll \hat{x}_c \ll \epsilon_n^{-1/2}$ is the boundary between the inner and intermediate regions. Note that if $J_c < 0$ (as will turn out to be the case) then the final term in Eq. (110) is *stabilizing*.

VI. NUMERICAL RESULTS

The scheme outlined in the previous section has been implemented numerically.

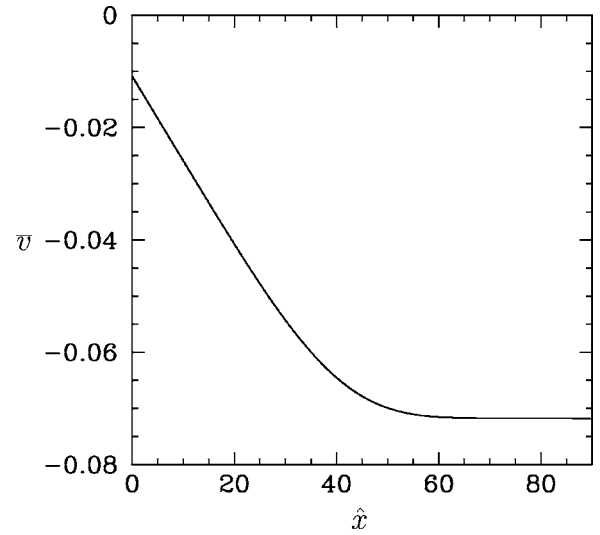Figures 1–4 illustrate the properties of a typical isolated

FIG. 2. The mean ion velocity profile $\bar{v}(\hat{x})$ in the intermediate region for the isolated island solution shown in Fig. 1.

(i.e., $\hat{v}'_\infty=0$) island solution. Figure 1 shows the ion fluid velocity profile $v(\hat{x},\theta)$ in the inner region. [Recall that the ion fluid velocity (normalized to the election diamagnetic velocity) in the island frame is $V_i = 1 + v(\hat{x},\theta)$.] It can be seen that the profile is completely *continuous*, and has a *finite gradient* at large $|\hat{x}|$. Figure 1 also shows the electron fluid velocity profile (normalized to the electron diamagnetic velocity), i.e., $V_e = G(\hat{x},\theta)$, through the island O-point (in the island frame). It is evident that the electron velocity profile is *discontinuous* across the island separatrix; i.e., it is zero inside, and finite immediately outside, the separatrix. Of course, this discontinuity in the electron fluid velocity profile could be resolved by adding a small amount of electron viscosity (i.e., hyperviscosity) to our model equations. Note, however, that the discontinuity does not give rise to a finite contribution to the ion polarization term in the Rutherford island width evolution equation (unlike the similar disconti-
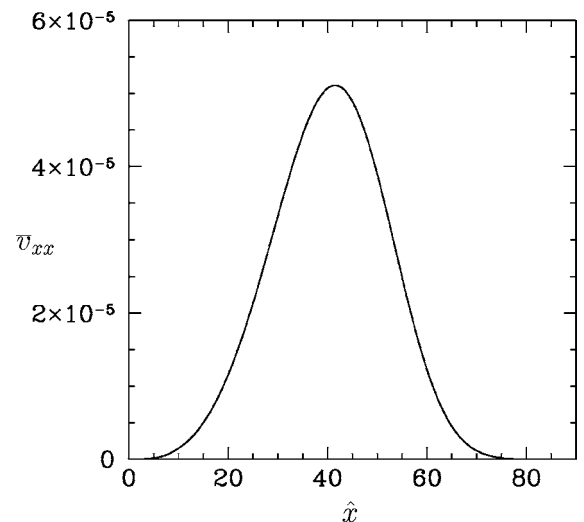

FIG. 3. The force density acting in the intermediate region due to the absorption of drift-acoustic waves emitted by the island, as parametrized by $\bar{v}_{xx}(\hat{x})$, for the isolated island solution shown in Fig. 1.
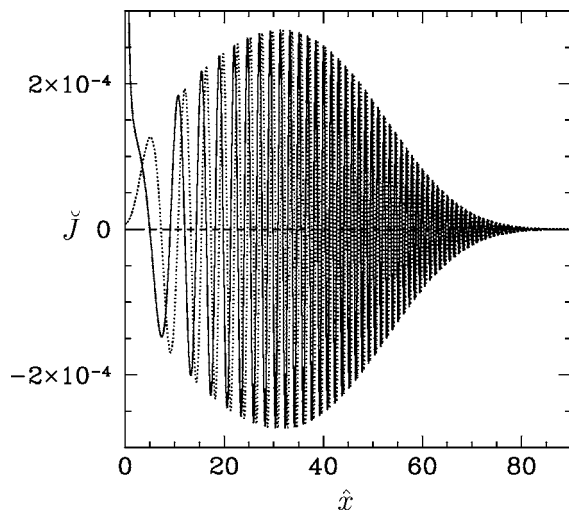
FIG. 4. The perturbed current density $\breve{J}$ in the intermediate region for the isolated island solution shown in Fig. 1. The solid and dotted curves show the real and imaginary parts of $\breve{J}$, respectively.

FIG. 6. The force parameter $\hat{v}'_\infty$ as a function of the flattening parameter v_0, for a series of island solutions characterized by $\epsilon_n=0.1$, $\hat{\mu}=0.001$, Sc$=1.0$, and the same value of $\hat{w}$. The solid curve shows the subcritical case $\hat{w}=0.1320$, whereas the dashed curve shows the supercritical case $\hat{w}=0.1322$.

nuity in the ion fluid velocity profile typically found in sonic island solutions[25]) because the electron fluid possesses negligible inertia. Figure 2 shows the mean ion fluid velocity profile in the intermediate region. It can be seen that the profile has *zero gradient* at large $|\hat{x}|$, as must be the case for an isolated island upon which no external force acts. Figure 3 shows the force density acting in the intermediate region due to the absorption of drift-acoustic waves emitted by the island, as parametrized by $\bar{v}_{xx}(\hat{x})$. This force density is responsible for reducing the finite gradient in the ion fluid velocity profile at the edge of the inner region to zero at the edge of the intermediate region. Finally, Fig. 4 shows the perturbed current density in the intermediate region. Observe that this current density decays to zero at the edge of the intermediate region.

Figure 5 shows the flattening parameter v_0 as a function of the island width parameter $\hat{w}$ for a series of isolated island solutions with the same values of ϵ_n, $\hat{\mu}$, and Sc. It can be
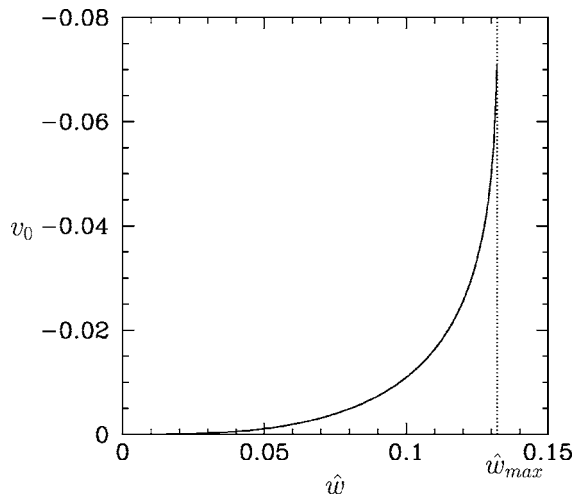

FIG. 5. The flattening parameter v_0 as a function of the island width parameter $\hat{w}$, for a series of isolated island solutions characterized by $\epsilon_n=0.1$, $\hat{\mu}=0.001$, and Sc$=1.0$.
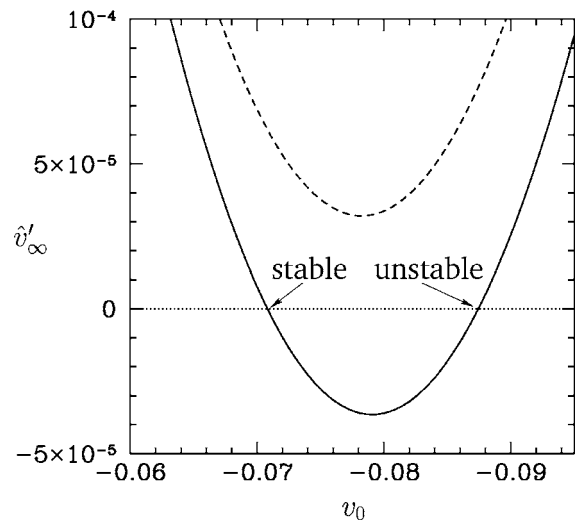
seen that v_0 is *negative*, indicating that sound-waves do indeed flatten, rather than steepen, the density profile inside the island separatrix. Note, however, that $|v_0|\ll 1$, which implies that the flattening effect is relatively small (recall that $v_0=0$ corresponds to no flattening, and $v_0=-1$ to complete flattening), as we would expect for a hypersonic island. According to Fig. 5, the magnitude of the flattening parameter increases rapidly with increasing island width. However, there exists a certain critical (normalized) island width $\hat{w}_{\max}$, above which there are no more solutions. Figure 6 demonstrates that this is a real effect, and not just a numerical artifact due, for instance, to any lack of convergence of our iterative solution method. Indeed, it can be seen from Fig. 6 that, below the critical island width, there are *two* isolated island solutions. These are indicated by the intersection of the force curve $\hat{v}'_\infty(v_0)$ with the horizontal axis. However, only one of these solutions (i.e., the one in which $\hat{v}'_\infty$ goes from being positive to negative as v_0 decreases) is *dynamical stable*. The other is *dynamically unstable*, and, therefore, unphysical. Above the critical island width, the force curve does not intersect the horizontal axis at all, and there are, thus, no isolated island solutions. It follows that the disappearance of our isolated island solution, as $\hat{w}$ increases, is a consequence of the convergence and mutual annihilation of the aforementioned stable and unstable island solutions.

Figure 7 demonstrates that the flattening parameter v_0 fits the scaling law

$$v_0 = -0.27\hat{w}^{+3.00}\epsilon_n^{+1.50}\hat{\mu}^{-1.00}\text{Sc}^{+1.00} \tag{113}$$

very well. The only deviation is at values of $|v_0|$ which are sufficiently large that $\hat{w}\to\hat{w}_{\max}$. Hence, the above scaling law holds whenever the island width lies significantly below the critical width.

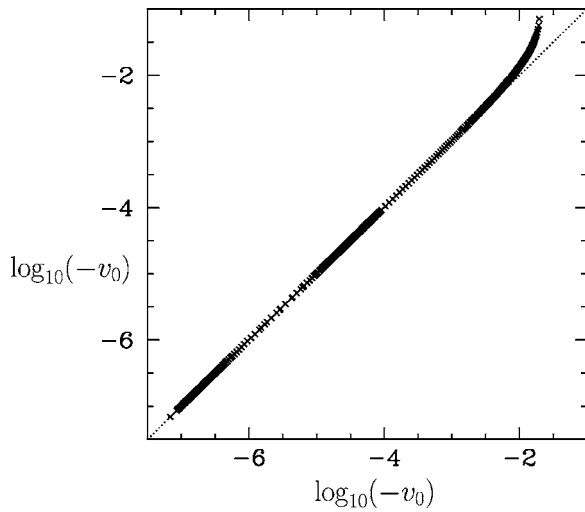Figure 8 demonstrates that the velocity parameter v_∞ fits the scaling law

FIG. 7. The flattening parameter v_0 (vertical axis) vs the scaling v_0 $=-0.27\hat{w}^{+3.00}\epsilon_n^{+1.50}\hat{\mu}^{-1.00}Sc^{+1.00}$ (horizontal axis) for a selection of isolated island solutions with $\hat{w}$ in the range 10^{-3} to 0.132, ϵ_n^2 in the range 10^{-3} to 10^{-1}, $\hat{\mu}$ in the range 10^{-3} to 10^{-1}, and Sc in the range 1.0 to 10.0.

$$v_\infty = -0.27\hat{w}^{+3.00}\epsilon_n^{+1.50}\hat{\mu}^{-1.00}Sc^{+1.00}$$
$$- 0.24\hat{w}^{+4.00}\epsilon_n^{+0.66}\hat{\mu}^{-1.33} \tag{114}$$

very well. Again, the only deviation is at values of $|v_\infty|$ that are sufficiently large that $\hat{w} \rightarrow \hat{w}_{max}$. Hence, the above scaling law also holds whenever the island width lies significantly below the critical width. Note that v_∞ is negative, indicating that the island propagation velocity lies between the unperturbed local electron and ion fluid velocities.

Figure 9 demonstrates that the stability parameter J_c fits the scaling law

$$J_c = -1.5\hat{w}^{+2.00}\epsilon_n^{+1.50} + 1.4\hat{w}^{+1.00}v_0^{+1.00} \tag{115}$$

very well. In this case, the scaling law holds even when $\hat{w} \rightarrow \hat{w}_{max}$. It can be seen from Eq. (110) that the first term on
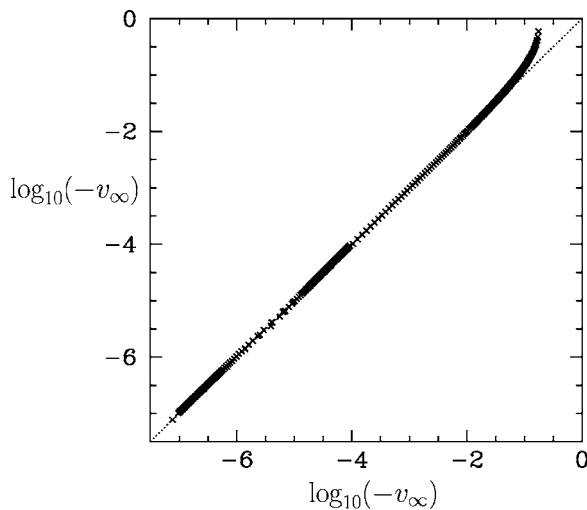
the right-hand side of the above scaling law gives rise to a *linear* stabilizing term in the Rutherford island width evolution equation of the form $-1.5\beta\epsilon_n^{-1/2}$. This term is due to coupling to drift-acoustic waves, and was first obtained analytically in Ref. 26. The fact that our numerical scheme exactly reproduces this analytic result indicates that our method of finding the outgoing wave solution in the intermediate region by damping drift-acoustic waves at large $|\hat{x}|$ (see Sec. IV B) is essentially correct. The second term on the right-hand side of the above scaling law gives rise to a *nonlinear* stabilizing term in the Rutherford island width evolution equation. This term is due to the ion polarization current generated by the slight flattening of the density profile inside the island separatrix.
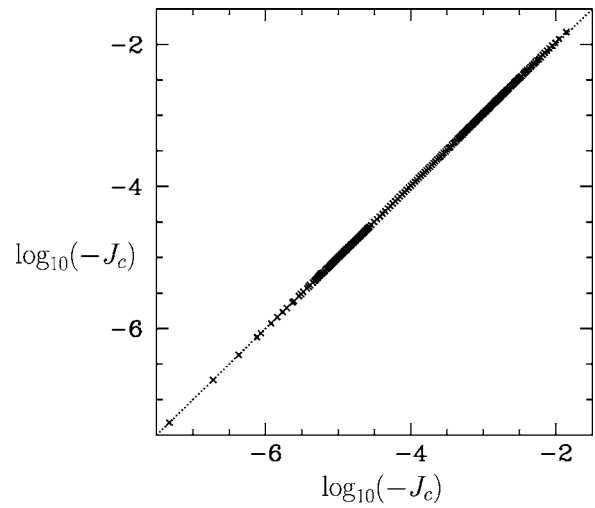
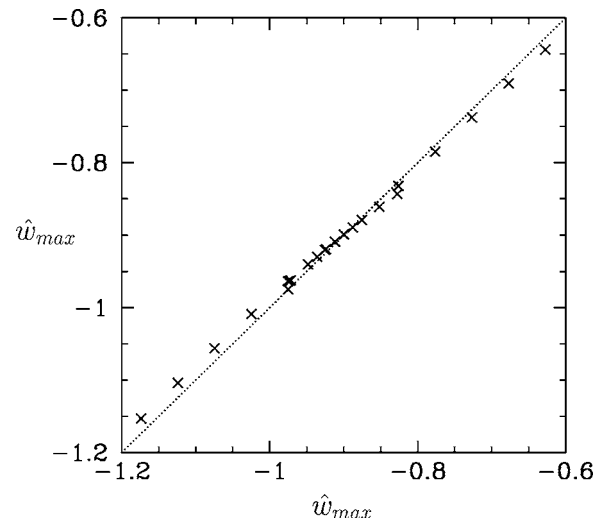Finally, Fig. 10 demonstrates that the maximum island

FIG. 9. The stability parameter J_c (vertical axis) vs the scaling J_c $=-1.5\hat{w}^{2.00}\epsilon_n^{1.50}+1.4\hat{w}v_0$ (horizontal axis) for a selection of isolated island solutions with $\hat{w}$ in the range 10^{-3} to 0.132, ϵ_n^2 in the range 10^{-3} to 10^{-1}, $\hat{\mu}$ in the range 10^{-3} to 10^{-1}, and Sc in the range 1.0 to 10.0.

FIG. 8. The velocity parameter v_∞ (vertical axis) vs the scaling v_∞ $=-0.27\hat{w}^{+3.00}\epsilon_n^{+1.50}\hat{\mu}^{-1.00}Sc^{+1.00}-0.24\hat{w}^{+4.00}\epsilon_n^{+0.66}\hat{\mu}^{-1.33}$ (horizontal axis) for a selection of isolated island solutions with $\hat{w}$ in the range 10^{-3} to 0.132, ϵ_n^2 in the range 10^{-3} to 10^{-1}, $\hat{\mu}$ in the range 10^{-3} to 10^{-1}, and Sc in the range 1.0 to 10.0.

FIG. 10. The maximum island width parameter $\hat{w}_{max}$ (vertical axis) vs the scaling $\hat{w}_{max}=0.9\epsilon_n^{-0.16}\hat{\mu}^{+0.33}Sc^{-0.33}$ (horizontal axis) for a selection of isolated island solutions with ϵ_n^2 in the range 2.5×10^{-3} to 0.16, $\hat{\mu}$ in the range 5×10^{-4} to 5.66×10^{-3}, and Sc in the range 1.0 to 8.0.

width parameter $\hat{w}_{\max}$ fits the scaling law

$$\hat{w}_{\max} = 0.9\epsilon_n^{-0.16}\hat{\mu}^{+0.33}\mathrm{Sc}^{-0.33} \tag{116}$$

to a reasonable approximation.

VII. SUMMARY AND DISCUSSION

By definition, *hypersonic* drift-tearing magnetic islands are too narrow for sound waves to effectively flatten the electron number density within the island separatrix. Such islands tend to propagate with a velocity close to that of the unperturbed local electron fluid. By contrast, *sonic* magnetic islands are sufficiently wide for sound waves to flatten the density within the separatrix, and tend to propagate with a velocity close to that of the unperturbed local ion fluid.

We have constructed a fully self-consistent theory of isolated, long-wavelength, hypersonic, drift-tearing magnetic islands in low-β, low-collisionality plasmas possessing relatively weak magnetic shear. The theory assumes both slab geometry and cold ions, and neglects electron temperature and equilibrium current gradient effects. The problem is solved in three asymptotically matched regions. The width of the inner region is of the order of the island width, which, in turn, is of the order of the ion sonic radius ρ_s. In the inner region, the problem boils down to a nonlinear second-order partial differential equation which can be solved via iteration (see Sec. III D). Note that the perturbed current does not go to zero at the edge of the inner region. The width of the intermediate region is of order $(L_s/L_n)^{1/2}\rho_s$. Here, L_s is the magnetic shear length, and L_n the density gradient scale-length. It is assumed that $L_n \ll L_s$. In the intermediate region, the problem reduces to a nonlinear second-order ordinary differential equation that can also be solved via iteration (see Sec. IV D). This equation describes how the island emits electrostatic drift-acoustic waves that propagate into the intermediate region, where they are absorbed by the plasma. Since the waves carry momentum, the inner region exerts a force on the intermediate region, and the intermediate region exerts an equal and opposite force on the inner region. One consequence of this force is the presence of a finite gradient in the ion fluid velocity profile at the edge of the inner region. The gradient in the ion fluid velocity profile is, of course, zero at the edge of the intermediate region, since the island is assumed to be isolated (i.e., there is assumed to be zero net external force acting on the island region). Hence, there is strong shear in the ion fluid velocity profile across the intermediate region (see Fig. 2). Finally, the perturbed current decays to zero at the edge of the intermediate region, allowing the island solution to be matched to a conventional linear ideal-MHD solution.

Our most important result is that the hypersonic branch of island solutions *ceases to exist* above a certain critical island width,[13,14] which we estimate to be

$$\hat{w}_{\max} = 0.9\epsilon_n^{-1/6}\hat{D}^{+1/3}, \tag{117}$$

where $\hat{w} = W/(4\rho_s)$, $\epsilon_n = L_n/L_s$, $\hat{D} = (D\tau_A/k\rho_s^3)/\hat{\beta}^{1/2}$, and $\hat{\beta} = \beta/\epsilon_n^2$. Here, W is the full island width, D the perpendicular particle diffusivity, τ_A the shear-Alfvèn time, k the island wave-number, and β (half) the plasma beta. Note that $\hat{D}^{1/2}$

$\ll \hat{w}_{\max} \ll \epsilon_n^{-1/2}$ (since our ordering scheme implies that $\hat{D} \ll \epsilon_n^2 \ll 1$). The significance of this inequality is that $\hat{D}^{1/2}$ is a typical linear layer width for the drift-tearing mode (normalized to ρ_s), whereas $\epsilon_n^{-1/2}$ is the width of the intermediate region (normalized to ρ_s). It follows that our hypersonic islands are typically much wider than a linear drift-tearing layer, but much narrower than the intermediate region, as has been assumed throughout this paper. Finally, if the island width exceeds the critical width then we hypothesize that there is a bifurcation to the sonic branch of solutions.[13,14]

The island phase velocity V_p is found to approximately satisfy

$$\frac{V_p - V_e}{V_e - V_i} = -0.27\hat{w}^3\epsilon_n^{3/2}\hat{D}^{-1} - 0.24\hat{w}^4\epsilon_n^{2/3}\hat{D}^{-4/3}\mathrm{Sc}^{-4/3}. \tag{118}$$

Here, V_i and V_e are the unperturbed local ion and electron fluid velocities, respectively. Moreover, $\mathrm{Sc} = \mu/D$, where μ is the perpendicular ion viscosity. Making use of Eq. (117), we can see that the maximum value of the first term on the right-hand side of the above equation is of order $\epsilon_n \ll 1$, whereas the maximum value of the second term is of order $\mathrm{Sc}^{-4/3}$. Since we have assumed, throughout this paper, that the island phase velocity lies relatively close to that of the unperturbed local electron fluid (which implies that the magnitude of the right-hand side of the above equation is much less than unity), it follows that when $\mathrm{Sc} \ll 1$, our theory breaks down at large island widths. However, there is no problem when $\mathrm{Sc} \gg 1$. The fact that the right-hand side of the above equation is negative implies that the island propagates *between* the velocities of the unperturbed local electron and ion fluids.

Finally, the Rutherford island width evolution equation is found to take the approximate form

$$\frac{dW}{dt} \propto \Delta'\rho_s - 1.5\beta\epsilon_n^{-1/2} - 0.38\beta\epsilon_n^{-1/2}\hat{w}^2\hat{D}^{-1}. \tag{119}$$

Here, Δ' is the linear tearing stability index. The final two terms on the right-hand side of the above equation represent the stabilizing influence of coupling to drift-acoustic waves, and the stabilizing influence of the ion polarization current, respectively. The former term is linear, and is well known.[24,26] The latter term, however, is nonlinear, and grows rapidly in magnitude as the island width increases. Indeed, this term dominates the linear term as soon as the island enters the nonlinear regime; i.e., as soon as $\hat{w} \gg \hat{D}^{1/2}$.

The analysis in this paper makes use of the constant-ψ approximation, which is valid provided that $|\Delta|\delta \ll 1$, where Δ is the jump in the logarithmic derivative of ψ across the nonideal MHD region, and δ is the width of this region. It follows, from the previous analysis, that $\delta \sim \epsilon_n^{-1/2}\rho_s$, and $\Delta\rho_s \sim \beta\epsilon_n^{-1/2}\hat{w}^2\hat{D}^{-1}$, with $\hat{w} \sim \epsilon_n^{-1/6}\hat{D}^{1/3}$. Hence, the constant-$\psi$ approximation is holds when $\hat{\beta}(\epsilon_n^2/\hat{D})^{1/3} \ll 1$. However, we have already assumed that $\hat{D} \ll \epsilon_n^2$. Thus, we require

$$1 \gg \frac{\hat{D}}{\epsilon_n^2} \gg \hat{\beta}^3. \tag{120}$$

Note that it is possible for the above condition to be satisfied, since $\hat{\beta} \ll 1$, by assumption.

One very interesting aspect of our hypersonic island solution is the presence of *strong velocity shear* in the region immediately surrounding the island (see Fig. 2). It is possible that this shear may become sufficiently large to quench plasma turbulence in the vicinity of the island.[24]

There are, of course, many important physical effects missing from our model. These include electron temperature and equilibrium current gradients, high-β effects, high-collisionality effects, ion diamagnetism, finite ion orbit widths, magnetic field-line curvature, neoclassical viscosity, ion Landau damping, and plasma turbulence. We shall attempt to incorporating some of these effects into our model in future publications.

ACKNOWLEDGMENTS

[1]H. P. Furth, J. Killeen, and M. N. Rosenbluth, Phys. Fluids **6**, 459 (1963).
[2]M. N. Rosenbluth, Plasma Phys. Controlled Fusion **41**, A99 (1999).
[3]P. H. Rutherford, Phys. Fluids **16**, 1903 (1973).
[4]Z. Chang and J. D. Callen, Nucl. Fusion **30**, 219 (1990).
[5]B. D. Scott, A. B. Hassam, and J. F. Drake, Phys. Fluids **28**, 275 (1985).
[6]B. D. Scott and A. B. Hassam, Phys. Fluids **30**, 90 (1987).
[7]A. I. Smolyakov, Plasma Phys. Controlled Fusion **35**, 657 (1993).
[8]A. B. Mikhailovskii, Contrib. Plasma Phys. **43**, 125 (2003).
[9]G. Ara, B. Basu, B. Coppi, G. Laval, M. N. Rosenbluth, and B. V. Waddell, Ann. Phys. (N.Y.) **112**, 443 (1978).
[10]J. F. Drake and Y. C. Lee, Phys. Fluids **20**, 134 (1977).
[11]R. D. Hazeltine and J. D. Meiss, Phys. Rep. **121**, 1 (1985).
[12]R. D. Hazeltine and J. D. Meiss, *Plasma Confinement* (Dover, Mineola, 2003).
[13]M. Ottaviani, F. Porcelli, and D. Grasso, Phys. Rev. Lett. **93**, 075001 (2004).
[14]R. Fitzpatrick, F. L. Waelbroeck, and F. Militello, Phys. Plasmas **13**, 122507 (2006).
[15]R. Fitzpatrick and F. L. Waelbroeck, Phys. Plasmas **12**, 122511 (2005).
[16]F. L. Waelbroeck, Plasma Phys. Controlled Fusion **49**, 905 (2007).
[17]R. D. Hazeltine, M. Kotschenreuther, and P. J. Morrison, Phys. Fluids **28**, 2466 (1985).
[18]J. W. Connor, F. L. Waelbroeck, and H. R. Wilson, Phys. Plasmas **8**, 2835 (2001).
[19]F. L. Waelbroeck, J. W. Connor, and H. R. Wilson, Phys. Rev. Lett. **87**, 215003 (2001).
[20]F. L. Waelbroeck, Phys. Rev. Lett. **95**, 035002 (2005).
[21]P. H. Rutherford, in *Basic Physical Processes of Toroidal Fusion Plasmas*, Proc. Course and Workshop, Varenna, 1985 (Commission of the European Communities, Brussels, 1986) Vol. 2, p. 531.
[22]J. F. Drake, J. T. M. Antonsen, A. B. Hassam, and N. T. Gladd, Phys. Fluids **26**, 2509 (1983).
[23]L. D. Pearlstein and H. L. Berk, Phys. Rev. Lett. **23**, 220 (1969).
[24]D. Grasso, M. Ottaviani, and F. Porcelli, Nucl. Fusion **42**, 1067 (2002).
[25]F. L. Waelbroeck and R. Fitzpatrick, Phys. Rev. Lett. **78**, 1703 (1997).
[26]M. N. Bussac, D. Edery, R. Pellat, and J. L. Soule, Phys. Rev. Lett. **40**, 1500 (1978).